Title

Membranes serve as allosteric activators of phospholipase A2, enabling it to extract, bind, and hydrolyze phospholipid substrates

Journal

Proceedings of the National Academy of Sciences of the United States of America, 112(6)

ISSN

0027-8424

Authors

Mouchlis, Varnavas D

Bucher, Denis

McCammon, J Andrew

et al.

Publication Date

2015-02-10

DOI

10.1073/pnas.1424651112

Peer reviewed

Membranes serve as allosteric activators of phospholipase A_2, enabling it to extract, bind, and hydrolyze phospholipid substrates

Varnavas D. Mouchlis[a,b,1], Denis Bucher[b], J. Andrew McCammon[a,b,c,1], and Edward A. Dennis[a,b,1]

Departments of [a]Pharmacology and [b]Chemistry and Biochemistry, and [c]Howard Hughes Medical Institute, University of California, San Diego, La Jolla, CA 92093-0601

Contributed by J. Andrew McCammon, December 30, 2014 (sent for review December 9, 2014; reviewed by Jeffry D. Madura)

Defining the molecular details and consequences of the association of water-soluble proteins with membranes is fundamental to understanding protein–lipid interactions and membrane functioning. Phospholipase A_2 (PLA_2) enzymes, which catalyze the hydrolysis of phospholipid substrates that compose the membrane bilayers, provide the ideal system for studying protein–lipid interactions. Our study focuses on understanding the catalytic cycle of two different human PLA_2s: the cytosolic Group IVA $cPLA_2$ and calcium-independent Group VIA $iPLA_2$. Computer-aided techniques guided by deuterium exchange mass spectrometry data, were used to create structural complexes of each enzyme with a single phospholipid substrate molecule, whereas the substrate extraction process was studied using steered molecular dynamics simulations. Molecular dynamic simulations of the enzyme–substrate–membrane systems revealed important information about the mechanisms by which these enzymes associate with the membrane and then extract and bind their phospholipid substrate. Our data support the hypothesis that the membrane acts as an allosteric ligand that binds at the allosteric site of the enzyme's interfacial surface, shifting its conformation from a closed (inactive) state in water to an open (active) state at the membrane interface.

GIVA $cPLA_2$ | GVIA $iPLA_2$ | PAPC | MD simulations | DXMS

During the last half century, much effort has been devoted to understanding how members of the phospholipase A_2 (PLA_2) enzyme superfamily interact with membranes. This takes on great importance because of the various biological functions associated with their ability to catalyze the hydrolysis of the ester bond at the *sn*-2 position of phospholipid molecules in membranes, liberating arachidonic acid (AA) and other polyunsaturated free fatty acids (PUFAs), as well as lysophospholipids (1). AA and other PUFAs are metabolic precursors for the biosynthesis of eicosanoids, including prostaglandins and leukotrienes, which are implicated in many inflammatory conditions (2). Through the eicosanoid pathways, PLA_2s have been implicated in many inflammatory diseases, including asthma, arthritis, atherosclerosis, pain, and cancer (3–5). There are 16 groups and many subgroups of PLA_2, but they can be considered as six types: cytosolic ($cPLA_2$), secreted ($sPLA_2$), calcium-independent ($iPLA_2$), platelet-activating factor acetylhydrolase (PAF-AH), also known as lipoprotein-associated PLA_2 ($Lp\text{-}PLA_2$), lysosomal PLA_2 ($LPLA_2$), and adipose-PLA_2 ($AdPLA_2$) (1). Among them, the two cytosolic water-soluble membrane-associated enzymes described in this study are implicated in numerous inflammatory and metabolic diseases (1, 6, 7). Thus, both enzymes are attractive targets for inhibitor development (8–10). However, there are no reported studies describing their interactions with a single phospholipid substrate molecule extracted from the membrane into the binding pocket of these enzymes.

The human Group IVA cytosolic PLA_2 (GIVA $cPLA_2$, $cPLA_2\alpha$) was cloned and sequenced from U937 cells in 1990 (11). This enzyme contains 749 amino acids and has a molecular weight of 85.2 kDa (12). Its X-ray crystal structure [Protein Data Bank (PDB) ID 1CJY; Fig. S1*A*] revealed an N-terminal C2 domain and a C-terminal α/β hydrolase catalytic domain (13). The GIVA $cPLA_2$ is regulated by intracellular calcium, which binds to a calcium binding site located on the C2 domain of the enzyme, resulting in the translocation of the enzyme to the surface of the phospholipid membrane (14). The enzyme is then able to access its phospholipid substrate, and uses a catalytic dyad of Ser/Asp to catalyze the hydrolysis (15). MAP kinase phosphorylation, as well as the lipid mediators ceramide-1-phosphate and phosphatidylinositol 4,5-bis phosphate, were shown to further enhance the activity of GIVA $cPLA_2$ (16–18). GIVA $cPLA_2$ exhibits high specificity for phospholipids containing AA at the *sn*-2 position (19).

The human Group VIA calcium-independent PLA_2 (GVIA $iPLA_2$, $iPLA_2\beta$) gene was found to express multiple splice variants (20). Among them, transcript variant 1 is the longer splice variant, containing 806 amino acids, and has a molecular weight of 89.9 kDa. The X-ray crystal structure of the enzyme has not been solved yet, but sequence alignment studies revealed seven ankyrin (ANK) repeats, a linker region, and an α/β hydrolase catalytic domain (20). The sequence of the human transcript variant 1 shows the insertion of an additional 54 amino acids, compared with the human transcript variant 2, which interrupts the eighth ANK repeat (20, 21). ANK repeats are often involved in protein–protein interactions regulating the activity of many enzymes (22). The human enzyme is similar to the earlier discovered murine $iPLA_2$ (23). GVIA $iPLA_2$ also uses a catalytic dyad of Ser/Asp; its catalytic activity is enhanced by ATP and does not show specificity for the *sn*-2 fatty acid (24).

Significance

The catalytic mechanisms of interfacial enzymes acting directly on the interfacial surface of the membrane are notoriously difficult to study experimentally with X-ray crystallography and other biophysical methods. This scientific study is, to our knowledge, the first to highlight similarities and differences in the extraction and binding of a phospholipid molecule into the substrate binding pocket of two human phospholipases A_2 (PLA_2s): the cytosolic Group IVA $cPLA_2$ and the calcium-independent Group VIA $iPLA_2$. Molecular dynamics simulations, guided by deuterium exchange experiments, are used to show that pathways to the active sites of these PLA_2s are opened upon allosteric interaction with the membrane to facilitate entry of the substrate lipid. These enzymes are involved in various diseases, and understanding their mechanisms will aid in the discovery of therapeutics.

Author contributions: V.D.M., D.B., J.A.M., and E.A.D. designed research; V.D.M. performed research; V.D.M., D.B., J.A.M., and E.A.D. analyzed data; and V.D.M., D.B., J.A.M., and E.A.D. wrote the paper.

Reviewers included: J.D.M., Duquesne University.

The authors declare no conflict of interest.

[1]To whom correspondence may be addressed. Email: vmouchlis@ucsd.edu, jmccammon@ucsd.edu, or edennis@ucsd.edu.

This article contains supporting information online at www.pnas.org/lookup/suppl/doi:10.1073/pnas.1424651112/-/DCSupplemental.

The PLA_2 catalytic cycle can be described in four steps: association of the enzyme with the membrane, extraction and binding of a single phospholipid molecule from the membrane into the binding pocket, hydrolysis, and product diffusion. The most critical step of the PLA_2 catalytic cycle is the association of the enzyme with the membrane through its interfacial binding region, which interacts with the membrane by means of electrostatic, hydrophobic, and hydrogen-bonding (H-bonding) interactions. Understanding the mechanistic details of how PLA_2s interact with membranes to access their substrate is a very challenging biological question that we have addressed in this study. Although several PLA_2 X-ray crystal structures have been published in the past, none of them contained cocrystallized natural phospholipid substrates or membranes. Hydrogen/deuterium exchange mass spectrometry (DXMS) (25) has been successfully used in the past to study PLA_2–substrate, –inhibitor, and –membrane interactions (26, 27). In this study, computer modeling and simulations have been used to interpret previously published DXMS data (28–31), in an effort to understand mechanistic questions related to the structural characteristics of GIVA $cPLA_2$ and GVIA $iPLA_2$. In particular, the extraction and binding of a single 1-palmitoyl-2-arachidonoyl-*sn*-glycero-3-phosphocholine (PAPC) phospholipid substrate into the binding pocket of these enzymes were studied using induced fit docking (IFD) (32) and steered molecular dynamics (SMD) simulations (33). Long molecular dynamics (MD) simulations were carried out to the enzyme–PAPC complexes in the presence of 1-palmitoyl-2-oleoyl-*sn*-glycero-3-phosphocholine (POPC) membrane patches using NAMD (33). The GIVA $cPLA_2$ has a strong preference for AA in the *sn*-2 position of the phospholipid substrate, which also serves as an optimal substrate for GVIA $iPLA_2$, although GVIA $iPLA_2$ is more permissive as to the fatty acid it hydrolyzes; thus for a direct comparison of the two enzymes, we used PAPC as substrate, as is typically done for kinetic comparisons. However, the most abundant and representative phospholipid in membranes is POPC, so this phospholipid was used for the membrane interaction studies. Our results provide insight into the binding of both enzymes with the PAPC substrate molecule and the POPC membranes, suggesting that the membrane is an important factor that should be taken into consideration in future computer-aided design efforts on PLA_2s.

Results

Homology Modeling and Sequence Alignment. In the absence of a crystal structure for GVIA $iPLA_2$, homology modeling is a powerful method to predict the 3D structure of enzymes on the basis of existing X-ray crystal structure templates. The method includes template identification, alignment, model building, and refinement. Prime 3.1 (34) was used to generate the homology model for GVIA $iPLA_2$ (Fig. S1*B*). The BLAST homology search was performed on the National Center for Biotechnology Information (NCBI) PDB database to identify the template. On the basis of the BLAST homology search, the sequence of GVIA $iPLA_2$ was separated into three regions: residues 1–120, for which no template was found; residues 121–474, which have 51% homology (similarity) with human ankyrinR (PDB ID 1N11) (22); and residues 475–806, which show 34% homology with patatin (PDB ID 1OXW) (35). This study focuses on the catalytic domain (residues 475–806), which contains the active site where the phospholipid substrate binds. According to the sequence alignment with patatin, the catalytic serine in GVIA $iPLA_2$ lies in a highly conserved lipase motif *GXSXG*.

Sequence alignment of the α/β hydrolase catalytic domain of GIVA $cPLA_2$ with the one of patatin and GVIA $iPLA_2$ shows only 20% homology, explaining why GIVA $cPLA_2$ belongs to the lysophospholipase family rather than the patatin-like family. Even though the homology is low, the lipase motif, the "dual signature nucleotide" (36), and the catalytic Asp motif are conserved in all three enzymes, with slight differences (Fig. 1). Alignment of the X-ray crystal structure of GIVA $cPLA_2$ with the one of patatin (rmsd of ∼4.0 Å and alignment score of ∼0.7) indicates that the folding of the α/β hydrolase catalytic domain is very similar (Fig. 1). In particular, the catalytic serine and the catalytic aspartic acid are located on two loops between a β-sheet and an α-helix, opposite one another, whereas the dual signature nucleotide (oxyanion hole with the Arg or Lys) is located on a similar loop under the catalytic serine (Fig. 1). Similar folding of GIVA $cPLA_2$ with patatin, even though the homology between them is very low, suggests that it is more likely that GVIA $iPLA_2$ and patatin have similar folding because the homology between them is higher.

Defining the Binding Pocket of the PLA_2 Enzymes. SiteMap 2.6 (37) was used to identify the binding pockets of GIVA $cPLA_2$ (crystal structure) and GVIA $iPLA_2$ (homology model), because both 3D structures of the enzymes exist in the apo form (no cocrystallized inhibitor or phospholipid), and the precise location of their binding pocket is not reported. SiteMap searches for suitable binding pockets by using grid points, called site points, and then uses the van der Waals and electrostatic interactions of a probe placed at each point to generate field maps. The probe simulates a water molecule with a van der Waals radius of 1.6 Å. SiteMap partitions the solvent accessible surface into three types of regions: hydrophobic, hydrophilic, and mixed character regions. The hydrophilic region is further divided into hydrogen-bond (H-bond) donor, H-bond acceptor, and metal-binding regions. The H-bond donor and acceptor properties indicate the degree to which a ligand might be expected to donate and accept H-bonds, respectively (37). The binding pocket with the highest SiteScore (1.114) in GIVA $cPLA_2$ (Fig. 2*A*) has a volume of ∼440 $Å^3$ and total solvent accessible surface of 1,453 $Å^2$. The hydrophobic region consists of 45% (magenta fields, Fig. 2*A*), the hydrophilic region of 30% (light blue fields, Fig. 2*A*), and the mixed character region 25% of the total surface. The hydrophobic region contains residues like Pro263, Phe295, Phe397, Phe681, and Phe683, whereas the hydrophilic region contains residues like Gly197, Gly198, Arg200, Ser228, Asp549, Asn555, Ser577, Glu588, and Lys589. The hydrophilic region is subdivided into H-bond donor and acceptor regions. The H-bond donor region consists of approximately 10% and the H-bond acceptor region approximately 20% of the hydrophilic region. The H-bond acceptor region refers to the degree that a well-structured ligand could interact with H-bond donor residues. The active site contains mostly H-bond donor residues like the catalytic Ser228, the oxyanion hole Gly197/Gly198, and Arg200. Because of the amphipathic character of the phospholipid molecules, hydrophilic head group, and hydrophobic fatty acid tails, there is a percentage of a mixed character region that might assist in its extraction into the binding pocket. The residues of the predicted binding pocket are part of the colored regions (Fig. 2*A*), which are

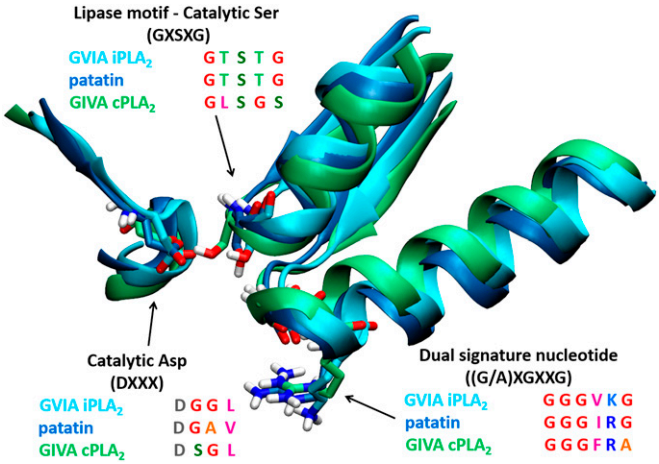

Fig. 1. Sequence and structure alignment of GVIA $iPLA_2$ (cyan), patatin (blue), and GIVA $cPLA_2$ (green).

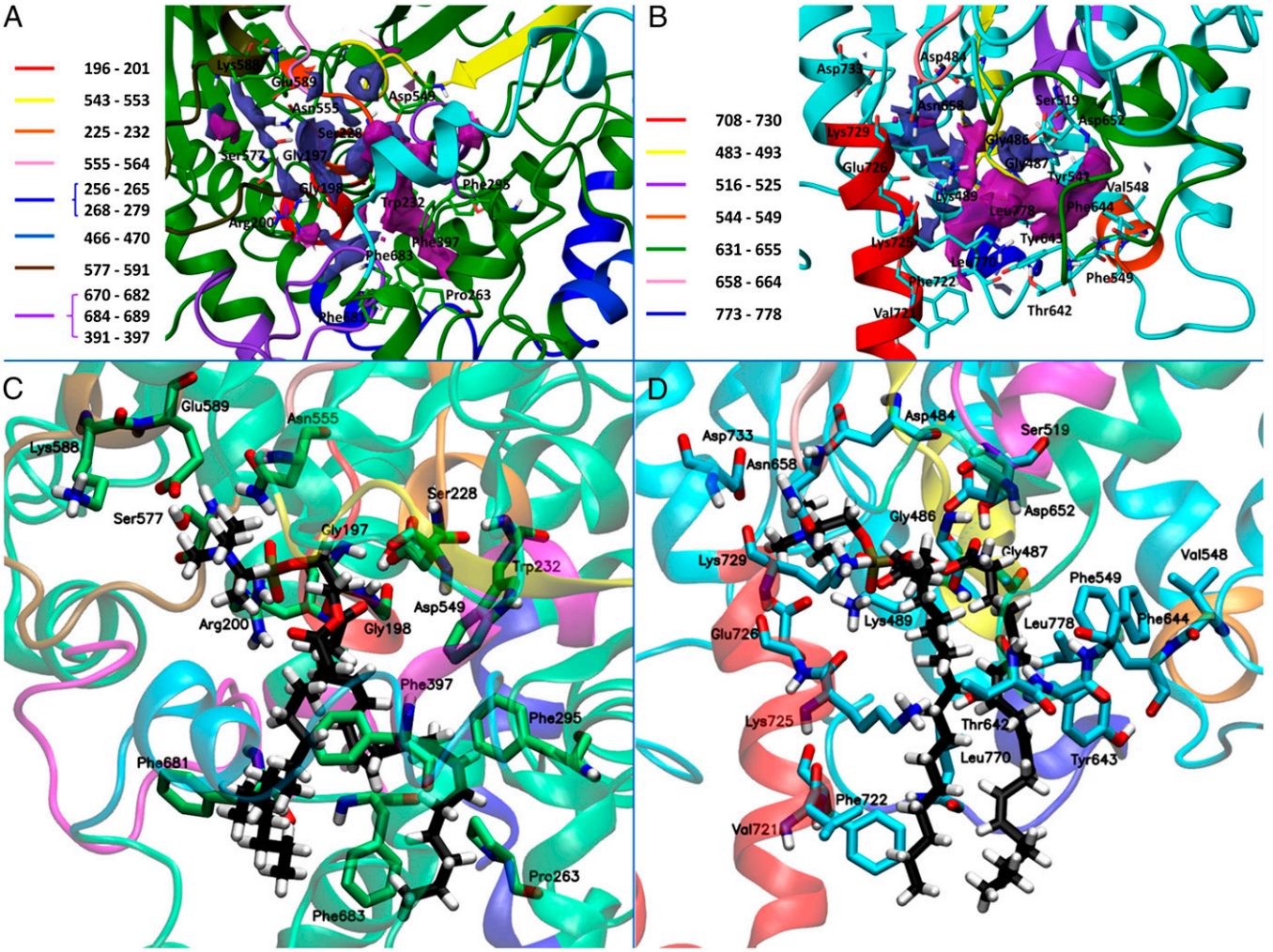

Fig. 2. Defining the binding pockets using SiteMap and predicting the PAPC–enzyme complexes using IFD for GIVA cPLA$_2$ and GVIA iPLA$_2$. (*A*) The binding pocket of GIVA cPLA$_2$, and (*B*) the binding pocket of GVIA iPLA$_2$: hydrophobic regions are highlighted in magenta and hydrophilic in light blue. (*C*) PAPC-GIVA cPLA$_2$ complex, and (*D*) PAPC-GVIA iPLA$_2$ complex predicted by IFD.

peptides found to interact with the substrate or inhibitor upon binding by DXMS experiments (30, 31). The close proximity of these regions to the predicted binding pocket supports its validity.

In GVIA iPLA$_2$, the binding pocket with the highest SiteScore (1.156; Fig. 2*B*) has a volume of ~355 Å^3 and a total solvent accessible surface of 1,486 Å^2. The percentage of the hydrophobic region (magenta fields, Fig. 2*B*) is 45%, the hydrophilic region (light blue fields, Fig. 2*B*) is 30%, and the mixed character region is 25%. The hydrophobic region contains residues like Val548, Phe549, Phe644, Val721, Phe722, Leu770, and Leu778. The hydrophilic region is also subdivided into 10% H-bond donor region and 20% H-bond acceptor region containing residues like Asp484, Gly486, Gly487, Lys489, Ser519, Asp652, Asn658, Lys725, Lys729, and Asp733. DXMS results from substrate and inhibitor binding studies (colored regions, Fig. 2*B*) also prove the validity of the predicted binding pocket (28, 29).

Predicting the PAPC–GIVA cPLA$_2$ and PAPC–GVIA iPLA$_2$ Structural Complexes. Although several studies have been reported in the literature describing the binding interactions of inhibitors with PLA$_2$s using X-ray crystallography or computational techniques (9), there have been no such studies on the binding interactions of phospholipid molecules. Our computational study was initially focused on the second step of the catalytic cycle, the binding of the phospholipid, because there are no available phospholipid–enzyme structural complexes to clearly determine the binding conformation and the interactions of the phospholipid with the residues of the pocket. The binding mode of the PAPC molecule in the pocket of each enzyme was predicted using two independent computational methods: first the IFD protocol implemented in the Schrödinger suite 2012 (32), and second SMD simulations using NAMD (33). The binding mode is defined as the binding conformation and the interactions of the PAPC molecule with the surrounding residues of the enzyme binding pocket.

PAPC–Enzyme Complexes Predicted by IFD Protocol. IFD is based on Glide 5.8 for the docking procedure and on Prime 3.1 for the refinement procedure and predicts ligand (in this study PAPC) binding modes and concomitant structural changes in the receptor. The representative complex was selected according to the XP score (approximately −8 kcal/mol), the conformation and orientation of PAPC, and its interactions with the binding pocket residues. In the two complexes (Fig. 2 *C* and *D*), the PAPC head group was placed in the hydrophilic region of the pocket, whereas the two fatty acid tails were placed in the hydrophobic region.

PAPC–Enzyme Complexes Predicted by SMD Simulations. SMD simulations are very useful in studying biological processes by accelerating the time scale accessible to MD simulations. Acceleration is achieved by applying an external force to part of the system, in

this study on the substrate (PAPC molecule), to lead it along a predefined direction (33). Although this introduces a bias in the system, equilibrium thermodynamic quantities such as the free energy profile or potential of mean force along the reaction coordinate can in principle be recovered from such study.

Even though GIVA $cPLA_2$ and GVIA $iPLA_2$ are water-soluble enzymes, they need to associate with the membrane to access their phospholipid substrate. Therefore, a model of the enzymes on a POPC membrane surface was used in the SMD simulations. A simplified model of GIVA $cPLA_2$ on the surface of the membrane was previously proposed on the basis of DXMS data (30). According to the model two regions of the C2 domain (residues 35–39 and 96–98) penetrate the membrane (~15 Å), leading the catalytic domain near the membrane surface. Two regions of the catalytic domain (residues 268–279 and 466–470; dark and light blue regions in Fig. 3*A*, respectively) are in close proximity to the surface of the membrane containing some hydrophobic residues (Trp464 and Met468; Fig. 3*A*) penetrating the membrane surface, and some hydrophilic residues (Lys273, 274, and Arg467) interacting with the head groups of the membrane. On the basis of the above information, the catalytic domain (residues 144–721) was embedded in a POPC membrane patch containing one PAPC molecule (Fig. 3*A*). The insertion of GVIA $iPLA_2$ in a POPC membrane patch was also previously studied by our group using coarse-grained and atomistic simulations, as well as DXMS data (38). The proposed model assumes no interactions of the ankyrin repeats with the membrane. One region of the catalytic domain (residues 708–730) penetrates the membrane, forming an amphipathic helix with its hydrophilic residues (Arg710, Lys719; Fig. 3*B*) interacting with the head groups, and its hydrophobic residues (Pro711, Pro714, Trp715, Leu717, Val721, Phe722; Fig. 3*B*) interacting with the fatty acid tails of the membrane phospholipid (38). GVIA $iPLA_2$ was also placed in the POPC membrane containing one PAPC molecule according to the published data (Fig. 3*B*).

The fully built models were equilibrated (*SI Materials and Methods*) and used as a starting point for the SMD simulations. PAPC was forced into the binding pockets of the enzymes using the constant velocity method of pulling, toward the direction shown in Fig. 3 *A* and *B* (thick black arrow). In SMD constant velocity simulations, the so-called SMD atoms (the atoms used for pulling) are attached to a dummy atom via a virtual spring, which is moved at constant velocity, and the force between them is measured (in this article the term "pulling force" was used) (33). To specify the parameters that better enforce the extraction of the PAPC molecule from the membrane into the enzyme binding pocket and ensure adequate sampling of the system, different velocities (3 Å/ns, 4 Å/ns, and 5 Å/ns) were tested with

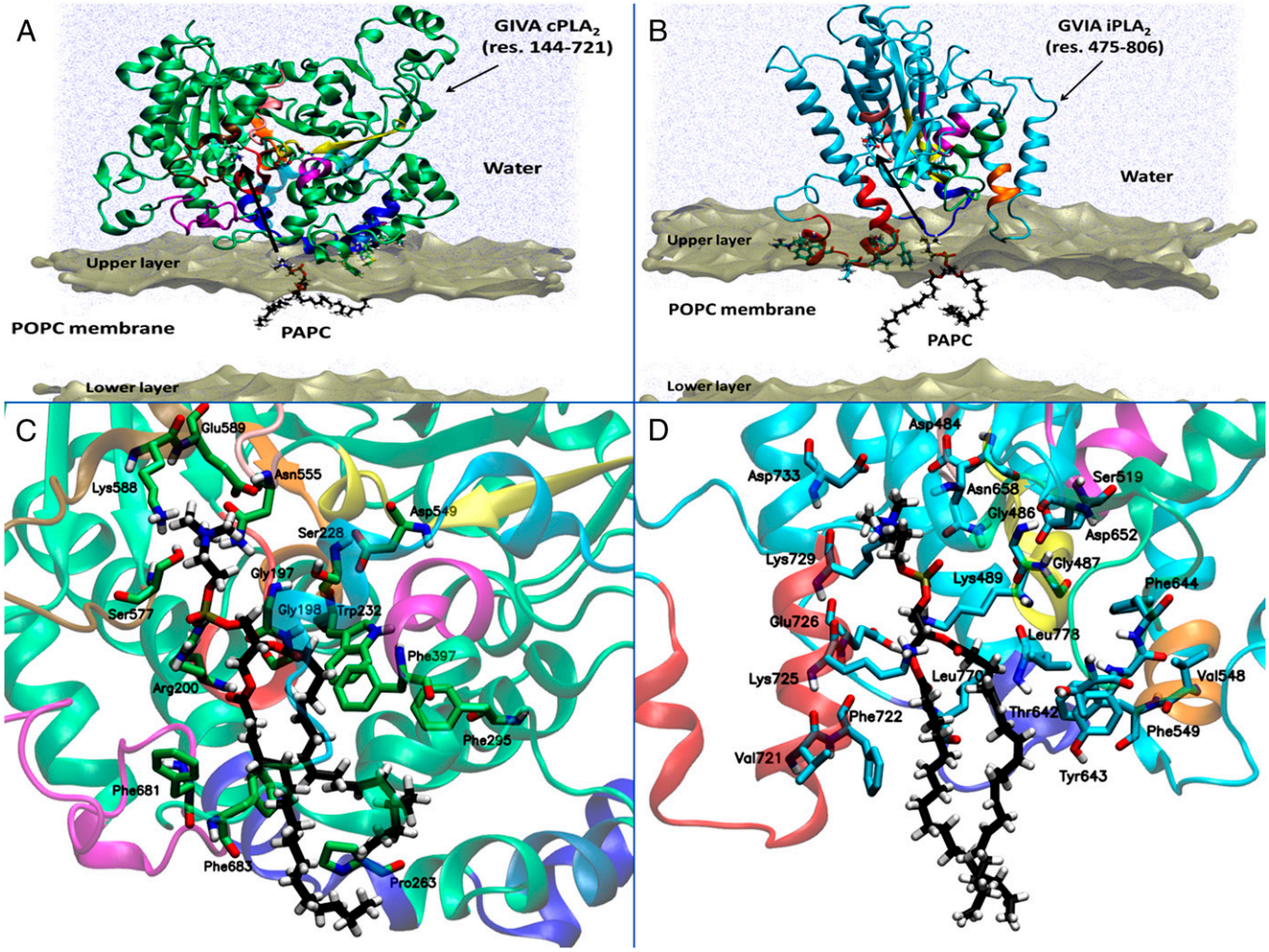

Fig. 3. Predicting the PAPC–enzyme complexes using SMD simulations for GIVA $cPLA_2$ and GVIA $iPLA_2$. (*A*) The system of GIVA $cPLA_2$ and PAPC embedded in a POPC membrane used for SMD simulations, in which the PAPC was pulled into the binding pocket in the direction depicted by the black arrow. (*B*) The system of GVIA $iPLA_2$ and PAPC embedded in a POPC membrane used for SMD simulations, in which the PAPC was pulled into the binding pocket in the direction depicted by the black arrow. (*C*) PAPC–GIVA $cPLA_2$ complex predicted by SMD (Movie S1). (*D*) PAPC–GVIA $iPLA_2$ complex predicted by SMD (Movie S2).

a force constant (k) of 10 kcal/mol*Å^2. For the preliminary SMD simulations the GVIA iPLA$_2$ was used. The position of PAPC during the time of the SMD simulations was calculated for all three simulations (Fig. S2 *A*–*C*). A constant velocity of 5 Å/ns indicated a smoother extraction of the PAPC molecule from the membrane into the enzyme pocket (Fig. S2*C*) and therefore was chosen for all of the SMD simulations in this study. The predicted SMD PAPC–enzyme complexes (Fig. 3 *C* and *D*) revealed a binding mode similar to the one predicted by IFD (Fig. 2 *C* and *D*) for both GIVA cPLA$_2$ and GVIA iPLA$_2$.

Two independent methods, the IFD protocol that incorporates partial receptor flexibility and the SMD simulations allowing full receptor flexibility, resulted in similar binding modes for PAPC in both enzymes, confirming the validity of the proposed complexes.

Binding Mode of PAPC in the Enzyme Binding Pocket. Even though the two binding modes predicted by IFD and SMD are very similar, the H-bonds in the complex predicted by IFD are more optimized. On the other hand, SMD gives full flexibility to both the PAPC and the enzyme, allowing them to relax and adopt a more optimized conformation in contrast to IFD that allows partial flexibility (backbone atoms fixed, side chains flexible) of the enzymes. The predicted orientation of the PAPC in the binding pocket is very similar in both IFD (Fig. 2 *C* and *D*) and SMD (Fig. 3 *C* and *D*) complexes, even though the fatty acid chains adopt different conformations due to high flexibility (rmsd of 4 Å). In particular, the PAPC head group was placed near the hydrophilic regions of the pocket (light blue fields in Fig. 2 *A* and *B*), with the phosphate group forming an H-bond with Arg200 in GIVA cPLA$_2$ and Lys489 in GVIA iPLA$_2$, in both IFD and SMD complexes. Arg200 and Lys489 are part of the dual signature nucleotide stabilizing the negatively charged phosphate group, not only through H-bonding but also through electrostatic interactions because they are positively charged. Another two residues, Asn555 in GIVA cPLA$_2$ and Asn658 in GVIA iPLA$_2$, are in close proximity with the phosphate group. The *sn*-2 carbonyl group of PAPC is participating in H-bonding with the oxyanion hole, Gly197/Gly198 in GIVA cPLA$_2$ and Gly486/Gly487 in GVIA iPLA$_2$. The *sn*-2 carbonyl group of PAPC is located near the catalytic Ser288 in GIVA cPLA$_2$ and Ser519 in GVIA iPLA$_2$ because it attacks the carbon atom of the PAPC *sn*-2 carbonyl group, forming a serine-acyl intermediate during the hydrolysis step of the catalytic cycle. The fatty acid tails of PAPC were placed in the hydrophobic regions of the binding pocket (magenta fields in Fig. 2 *A* and *B*) of each enzyme in both IFD (Fig. 2 *C* and *D*) and SMD (Fig. 3 *C* and *D*) complexes. In general, the fatty acid tails in GIVA cPLA$_2$ interact with residues like Trp232, Pro263, Phe295, Phe397, Phe681, and Phe683 located on regions showing changes in on-exchange rates in DXMS binding studies (colored regions in Figs. 2 *A* and *C* and 3*C*). In GVIA iPLA$_2$, the fatty acid tails interact with residues like Val548, Phe549, Phe643, Phe644, Val721, Phe722, Leu770, and Leu778 also located on regions showing decreases in on-exchange rates in DXMS studies (colored regions in Figs. 2 *B* and *D* and 3*D*).

Extraction of PAPC from the Membrane into the Binding Pocket. SMD has been successfully used in the past to address substrate binding and transport in water channels (39, 40). In this study, SMD revealed interesting information about the extraction process of a single PAPC substrate molecule from the membrane into the pocket of each enzyme and the associated role that various residues as well as the membrane play during the extraction for GIVA cPLA$_2$ (Movie S1) and for GVIA iPLA$_2$ (Movie S2).

In the case of GIVA cPLA$_2$, three regions are located near the entrance of the pocket: residues 261–268, 405–415, and 670–686. These regions contain residues like Asn268, Ser408, Gln411, Asn682, and Gln684, which interact with the PAPC molecule through H-bonding (broken yellow lines in Movie S1) during its extraction into the binding pocket (Movie S1). Arg200 is part of the dual signature nucleotide, and in the absence of the PAPC molecule interacts with Ser680 and Glu418. When the PAPC enters the active site approximately two-thirds of its length, Arg200 interacts with the phosphate group through H-bonding and electrostatic interactions, stabilizing its binding into the pocket of the enzyme. Glu418 is part of the lid (cyan region) that exhibits flexibility, whereas the PAPC enters the binding pocket. After the complete accommodation of the PAPC into the pocket, Glu418 and Glu589 are located near to the choline group, stabilizing its binding through electrostatic interactions. Finally, the two fatty acid tails are accommodated in the hydrophobic region of the pocket, with the *sn*-2 carbonyl group located near the oxyanion hole (Gly197/Gly198) and the four double bonds in close proximity with the aromatic residues Trp232, Phe295, Phe397, Phe681, and Phe683.

The SMD simulation of GVIA iPLA$_2$ also shed light on the extraction of a single PAPC molecule into the enzyme pocket (Movie S2). Two regions (residues 720–730 and 640–648) seem to play a significant role on the PAPC extraction. In particular, region 640–648 contains Thr642 and Tyr643, which seem to serve as gate keepers controlling the volume of the binding pocket. While PAPC enters the pocket, Tyr643 interacts through H-bonding with the phosphate group to help the extraction process. After PAPC reached Lys489, which is part of the dual signature nucleotide, it participates in H-bonding and electrostatic interactions with the phosphate. The phosphate group flips into the pocket, where it is stabilized by Lys489. On region 720–730, another residue, Lys725 also plays an important role in the extraction process by interacting with the *sn*-1 carbonyl group. Lys725 is also in close proximity with the phosphate group and seems to participate in H-bonding and electrostatic interactions, assisting further the extraction of PAPC into the pocket. The choline group was seen to repel Lys729 away from the pocket, locating itself near the negatively charged residues Asp733 and Asp484, which stabilize its binding through electrostatic interactions. Likewise, the two fatty acid tails are accommodated in the hydrophobic region of the pocket, with the *sn*-2 carbonyl group located near the oxyanion hole (Gly486/Gly487), but they are relatively exposed to the solvent.

MD Simulations of PAPC–Enzyme Complexes. MD simulations are an important computational tool widely used in understanding the dynamic properties of biological macromolecules associated with their biological function (41). DXMS is also a powerful technique used in understanding biological processes, including ligand binding, membrane association, and conformational changes (27). This experimental technique can be effectively combined with MD simulations to better address questions related to conformational changes that occur on PLA$_2$ enzymes when they function on the surface of the membrane (28–31).

The complexes of PAPC with GIVA cPLA$_2$ (X-ray structure) and GVIA iPLA$_2$ (homology model) predicted by IFD were initially placed on the surface of a POPC membrane patch, and the PAPC–enzyme–membrane system was subsequently placed in water ("explicit water model") in the presence of 100 mM sodium chloride. The two systems were equilibrated (*SI Materials and Methods*) and then subjected to 300-ns MD simulations. The coordinates extracted from the SMD simulations were also first equilibrated, to ensure stability of the complex, before conducting 300 ns of MD simulations. The structures and conformational flexibility observed in these two independent simulations were very similar, and therefore we will mainly discuss the trajectories of the simulations initiated from the IFD complexes, with frequent references to the trajectories of the SMD complexes. To identify the most populated conformation, the frames of each trajectory were clustered using the clustering plugin in VMD with an rmsd (all heavy-atom) cutoff of 2.0 Å (42). Among the five conformation clusters obtained, the most populated represented ~70% of the weight and was chosen as the most representative structure for the enzyme–PAPC complex.

Each simulation was performed in the *NPT* ensemble, and the rmsd of the protein backbone atoms over the time of the simulation was calculated to ensure that each system had equilibrated.

In the simulation of the GIVA cPLA$_2$–PAPC IFD complex, the rmsd for the enzyme backbone atoms was stabilized at ∼2 Å relative to the starting structure (green curve in Fig. S3*A*), whereas in the simulation of GIVA cPLA$_2$-PAPC SMD the rmsd was stabilized at ∼2.5 Å relative to the starting structure (blue curve in Fig. S3*A*). In both simulations the proposed enzyme–PAPC final complexes do not deviate much from each other, leading to a very similar enzyme conformation and PAPC binding mode (Fig. S3*C*; the structures are colored according to the curve color). All heavy-atom–based alignment of the enzyme final complex conformations gave an rmsd of ∼2.7 Å, indicating that the two conformations are very similar, whereas all heavy-atom–based alignment of the PAPC final complex conformations gave an rmsd of ∼1.7 Å, also showing that the two conformations are very similar.

The rmsd in the simulation of the GVIA iPLA$_2$–PAPC IFD complex was stabilized at ∼3.9 Å relative to the starting structure (cyan curve in Fig. S3*B*), whereas in the simulation of the GVIA iPLA$_2$–PAPC SMD complex the rmsd was stabilized at ∼4 Å (blue curve in Fig. S3*B*). The fact that the conformation of the enzyme in simulations of GVIA iPLA$_2$ was stabilized around an rmsd of ∼4 Å, which is ∼2 Å more than the ones in simulations of GIVA cPLA$_2$, might be either because the homology model needs more time to equilibrate and reach a potential energy local minimum or because the catalytic domain of GVIA iPLA$_2$ exhibits higher flexibility than the one of GIVA cPLA$_2$. Similarly to the simulations of GIVA cPLA$_2$–PAPC complexes, the ones on GVIA iPLA$_2$–PAPC complexes led to a very similar proposed final complex in terms of enzyme conformation and PAPC binding mode (Fig. S3*D*; the structures are colored according to the curve color). Likewise, all heavy-atom–based alignment of the enzyme final complex conformations gave an rmsd of ∼2.5 Å, whereas all heavy-atom–based alignment of the PAPC final complex conformations gave an rmsd of ∼2.4 Å.

Two independent simulations of GIVA cPLA$_2$ and GVIA iPLA$_2$—the first on the IFD and the second on the SMD enzyme–PAPC complex—yielded similar final conformations for the enzyme and PAPC binding modes, supporting the validity of the proposed structural complexes.

PAPC Binding Mode After the MD Simulations. Although the complexes predicted by IFD and SMD provided important information about the binding mode of the PAPC in each enzyme binding pocket, the MD simulations revealed further conformational adjustments of the enzyme-PAPC initial complexes, which led to an optimized binding mode (Fig. 4 *A* and *B* and Movies S3 and S4).

The fatty acid tails of the PAPC in GIVA cPLA$_2$ move into a small hydrophobic cavity located near the main binding pocket (Fig. 4*A*). This small cavity contains two peptides, residues 268–279 (blue region in Fig. 4*A*) and 466–470 (light blue region in Fig. 4*A*), which according to DXMS experiments exhibited a decrease in on-exchange rates in the presence of phospholipid vesicles (30). These amphipathic peptides are part of two helices playing a dual role because their exterior surface contains hydrophobic and hydrophilic residues helping in the association of the GIVA cPLA$_2$ catalytic domain with the membrane, and their interior surface contains hydrophobic and aromatic residues like Val272, Tyr275, Val276, Phe291, Phe401, Leu405, and His466, which interact with fatty acid tails of PAPC (Fig. 4*A*). The deep channel binding pocket of GIVA cPLA$_2$ can accommodate the PAPC molecule in its entirety. Three main H-bonds were observed during the simulation: two between Arg200 and Asn555 and the phosphate group, and one between the oxyanion hole (Gly197/Gly198) and the *sn*-2 carbonyl group. Fig. 4*C* shows the average number of H-bonds that the PAPC formed with the binding pocket during the time of the simulation (green curve). These three H-bonds were maintained during the first 150 ns of the simulation, whereas one H-bond with Arg200 was mainly formed during the next 100 ns, and finally two H-bonds with Arg200 and Asn555 were mainly observed for the last 50 ns. The catalytic dyad of Ser228/Asp549 interacts with each other, and with a water molecule that penetrates into the binding pocket (Movie S3).

The MD simulations of GIVA cPLA$_2$–PAPC complex revealed interesting information about the dynamic nature of the enzyme binding pocket. Root mean square fluctuation (rmsf) data showed two loops controlling the entrance of the deep channel binding pocket (regions A and B in Fig. S4*A*). These two loops contain predominantly hydrophilic residues like Ser410, Gln411, Thr680, and Gln684 that exhibit high flexibility, with rmsf more than 4 Å (Fig. S4 *B* and *C*). The role of region B (residues 408–414) is dual, because it also constitutes one of the hinges that control the movement of the lid (residues 415–432), with the other hinge region C (residues 433–457) showing high flexibility too (rmsf > 4 Å in Fig. S4*B*). The Lid itself shows intermediate flexibility, with its exterior surface containing acidic residues including Glu418 and Glu419, and its interior surface containing hydrophobic residues like Met417, Leu421, and Ile424 that interact with PAPC. Another flexible region near the binding pocket is D (Fig. S4*D*). This region contains Ser577 and Glu589 that interact periodically with PAPC. Lys588 constantly forms H-bonds with Glu418, which is located on the Lid, keeping the interior hydrophobic surface of the Lid near to the PAPC molecule (Fig. 4*A* and Movie S3). The information revealed by the MD simulations helps us to better understand the role that various peptide regions play in the binding of PAPC, including regions A and D that showed decreases in on-exchange rates in our published DXMS experiments on GIVA cPLA$_2$ (30, 31).

In the case of GVIA iPLA$_2$ regions A and B (Fig. S5*A*), which were reported to exhibit a decrease in on-exchange rates in DXMS experiments in the presence of phospholipid vesicles (29), they showed high and intermediate flexibility, respectively. The rmsf values for region A (residues 700–719) were higher than 4 Å (Fig. S5*B*), and it was previously reported to play an important role in the association of the enzyme with the membrane (38). Region B (residues 720–730) exhibited rmsf values between 1.5 Å and 4 Å (Fig. S5*B*), and it plays an important role in the extraction (see *Discussion*) and binding of the PAPC molecule. For instance, Val721 and Phe722 interact with the *sn*-1 fatty acid tail, whereas Lys729 participates in an H-bond either with the phosphate group or the *sn*-1 carbonyl group of PAPC (Fig. 4*B* and Movie S4). Regions C, D, and E (Fig. S5*A*) showed also high flexibility (Fig. S5 *C*–*E*), containing peptides that exhibited decreases in on-exchange rates in our previously published DXMS experiments (28, 29). All of the above regions have an amphipathic character because they act near to the membrane surface and are highly flexible, controlling the entrance to the binding pocket (Fig. S5*A*).

The binding pocket of GVIA iPLA$_2$ does not seem as deep as the one in GIVA cPLA$_2$. When the GIVA cPLA$_2$–PAPC complex was placed on the surface of the membrane patch containing POPC, and during the MD simulations, the PAPC molecule did not show any contact with the POPC molecules of the membrane patch, because it can be completely accommodated in the deep channel binding pocket of the enzyme (Fig. S6*A* and Movie S5). On the contrary, placement of the GVIA iPLA$_2$–PAPC complex on the surface of the membrane patch showed that the fatty acid tails of the PAPC molecule are in contact with the POPC molecules of the membrane patch (Fig. S6*B*). During the MD simulation of the GVIA iPLA$_2$–PAPC complex, the *sn*-2 fatty acid tail of PAPC becomes separated from the *sn*-1 fatty acid tail and is accommodated in the hydrophobic region of the enzyme interacting with residues including Tyr541, Val548, Phe549, Ile523, Tyr643, and Phe644 (Fig. 4*A* and Movie S4). The simulation revealed a synergy between GVIA iPLA$_2$ and the equilibrated POPC membrane during the binding of the PAPC molecule, showing that the POPC molecules assist in the separation of the *sn*-2 chain (Movie S6). The same synergy was not observed during the simulation of the GIVA cPLA$_2$–PAPC complex (Movie S5). Three H-bonds were observed for the first 150 ns of the simulation (Fig. 4*C*): two between Lys489 and Asn658 and the PAPC phosphate group, and one between the oxyanion hole (Gly486/Gly487) and the *sn*-2 carbonyl group. For the last 150 ns of the simulation

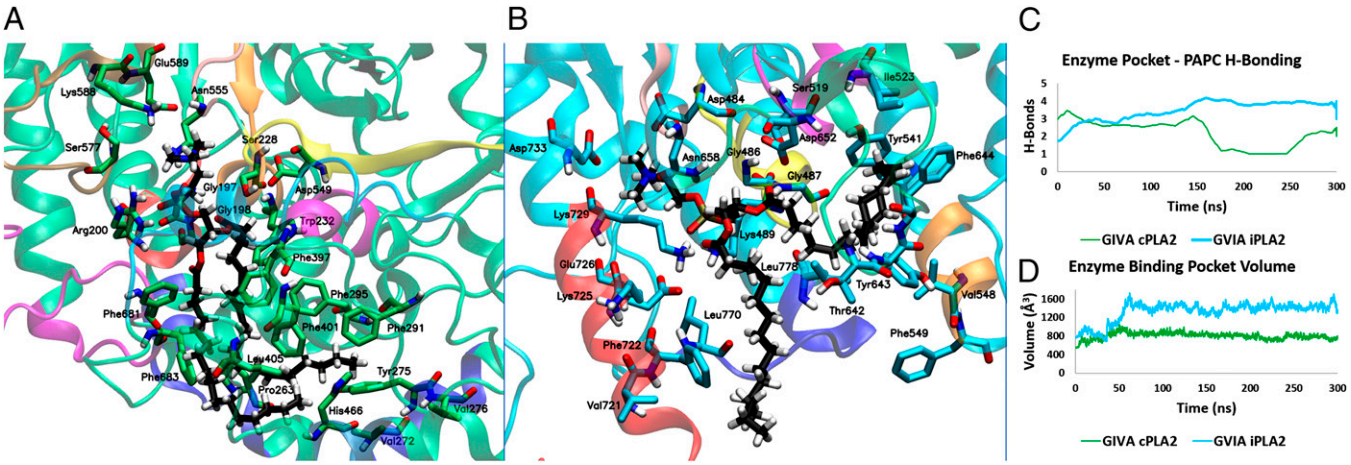

Fig. 4. PAPC binding mode, number of H-bonds, and volume of the binding pocket for GIVA cPLA$_2$ and GVIA iPLA$_2$ after 300-ns MD simulation. (*A*) Binding mode of PAPC in the GIVA cPLA$_2$ binding pocket (Movie S3). (*B*) Binding mode of PAPC in the GVIA iPLA$_2$ binding pocket (Movie S4). (*C*) Average number of H-Bonds of the PAPC with the residues of the binding pocket for each enzyme during the simulation. (*D*) Volume of the binding pocket of each enzyme during the simulation (Movies S7 and S8).

one more H-bond was observed between Lys729 and either the phosphate group or the *sn*-1 carbonyl group, increasing the average number of H-bonds to four (Fig. 4*C*). Similar to the simulation of GIVA cPLA$_2$, in the simulation of GVIA iPLA$_2$ the catalytic dyad of Ser519/Asp652 interacts with each other, and with a water molecule that penetrates into the binding pocket (Movie S4).

The Dynamic Nature of the Binding Pocket. Measuring the volume of the binding pocket during the MD simulations can give significant information about its dynamic nature by monitoring variations of the pocket size when multiple conformations of the same enzyme are considered. The volume of the binding pocket was measured with the Pocket Volume Measure (POVME) algorithm (43).

The binding pocket of GIVA cPLA$_2$ did not demonstrate a significant increase or fluctuations of its volume during the MD simulation. In particular, the volume was increased from ∼600 Å^3 (Fig. S7*A*) in the enzyme–PAPC initial complex to ∼800 Å^3 (Fig. S7*C*) during the first 50 ns, and it remained stable for the rest of the simulation (Fig. 4*D*, green curve, and Movie S7). The small increase of the binding pocket volume is associated with the accommodation of the two fatty acid tails into the previously mentioned small hydrophobic cavity located near the main binding pocket (Fig. S7*C*).

A significant increase of the binding pocket volume in the case of GVIA iPLA$_2$ suggested higher flexibility of the pocket in comparison with the one of GIVA cPLA$_2$. The volume was ∼700 Å^3 (Fig. S7*B*) in the enzyme–PAPC initial complex, and it was increased to an average of ∼1,400 Å^3 (Fig. S7*D*) during the first 60 ns of the simulation (Fig. 4*D*, cyan curve, and Movie S8). Compared with the binding pocket volume of GIVA cPLA$_2$, the GVIA iPLA$_2$ binding pocket volume exhibited a much higher increase and fluctuations (Fig. 4*D*) related to the accommodation of the *sn*-2 fatty acid tail into the hydrophobic region of the pocket (Fig. S7*D*).

According to the above conclusions, we hypothesize that GVIA iPLA$_2$ exists in an equilibrium between a closed (in water) and an open state (on the membrane and with a phospholipid molecule in the binding pocket). To further validate this hypothesis the PAPC substrate was removed from the enzyme binding pocket of the GVIA iPLA$_2$–PAPC complex, and the enzyme in its open state was used to run two 300-ns simulations: one in the presence of a POPC membrane and the other in the presence of water. Fig. 5 shows the binding pocket volume during the MD simulation of the GVIA iPLA$_2$–PAPC complex (cyan curve, Fig. 5*D*), for the open state without the PAPC, in the presence of a POPC membrane (brown curve, Fig. 5*D*), and in water (blue curve, Fig. 5*D*). It is remarkable that the volume of the pocket in the presence of the water (blue curve) shows higher fluctuations contrary to the simulations in the presence of PAPC (cyan curve) and POPC (brown curve), which could be explained by the decreased stability of the open state of the enzyme in the water. Indeed, we observe that the enzyme is adjusting its conformation to close the hydrophobic pocket, which has become exposed to the solvent. At the end of the simulations, the protein has transitioned from the open to the closed state in the presence of the water (Fig. 5*C*), whereas it remains open in the presence of the POPC membrane (Fig. 5*B*). A small decrease of the pocket size in the presence of POPC is associated with the closing of a small cavity that binds the choline group in the presence of PAPC (Fig. 5*A*).

DXMS also indicates that two peptide regions seem to play an important role in controlling the volume of the binding pocket, residues 640–648 and 720–730. These two regions showed a high decrease in on-exchange rates in DXMS in the presence of phospholipid vesicles (29). Region 640–648 is an amphipathic loop (color-coded loop in Movie S9) located near to the membrane surface, and exhibits high fluctuations during the MD simulations. Amphipathic character is typical for regions acting at the interface between membrane-water, and they usually contain mixed hydrophilic and hydrophobic residues. We postulate that three residues Thr642, Tyr643, and Phe644 serve as gatekeepers (44) for GVIA iPLA$_2$, controlling the volume of the pocket and participating in its opening and closing. When the membrane is present (brown color in Movie S9) the loop remains open with these three residues in spatial proximity with the surface of the membrane. In the absence of the membrane (blue color in Movie S9) these three residues move into the interior of the pocket to prevent water molecules from entering its hydrophobic region. In the presence of PAPC in the binding pocket, these three residues are interacting with the bound phospholipid (cyan color in Movie S9, and Movie S4).

The second region, residues 720–730, is a helix (color-coded helix in Movie S9) that also shows amphipathic character, contributing to the binding of the enzyme to the surface of the membrane (38) as well as to the extraction and binding of a single phospholipid molecule into the pocket (see *Discussion*). According to the MD simulations, this region also plays a significant role in controlling the volume of the binding pocket. Lys729, for instance, seems to stabilize a small cavity that contains negatively charged residues like Asp733 and Asp484. In the presence of a PAPC molecule in the pocket, this cavity binds the positively charged choline group, whereas in the absence of PAPC, Lys729

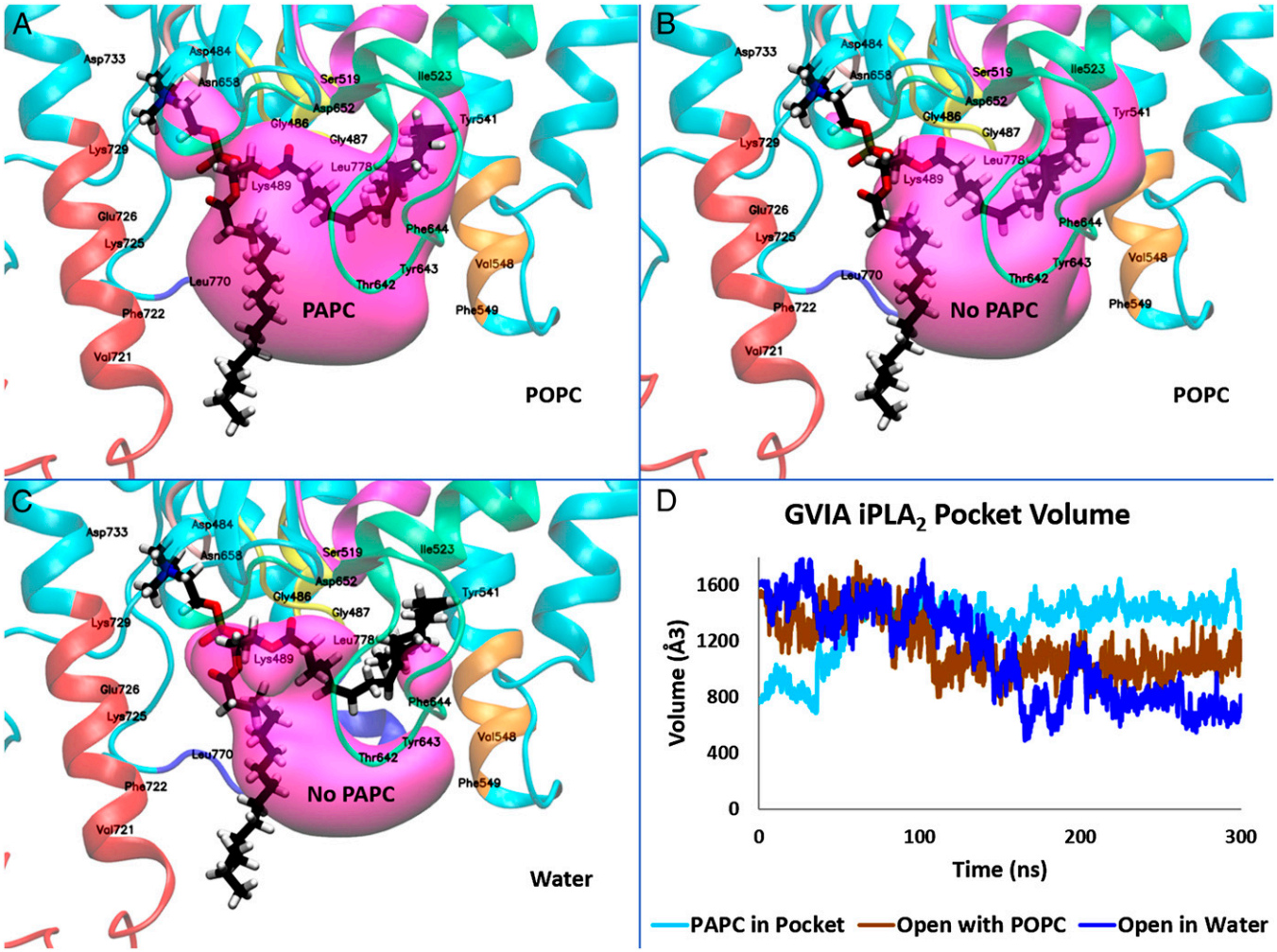

Fig. 5. The dynamic nature of the GVIA iPLA$_2$ binding pocket. Volume of the binding pocket during the MD simulation of (*A*) the GVIA iPLA$_2$-PAPC complex, (*B*) the open state without PAPC in the pocket (although PAPC is superimposed for visual convenience) in the presence of a membrane patch containing POPC, (*C*) the open state without PAPC (although PAPC is superimposed for visual convenience) in the pocket in the presence of water. (*D*) Volume of the binding pocket during the MD simulation (A, cyan; B, brown; and C, blue; Movie S9).

flips into the cavity interacting with its residues through H-bonding and electrostatic interactions (Movie S9). During the extraction, the choline group replaces Lys729, which in turn interacts with the phosphate group, stabilizing its binding in the pocket (Movies S2 and S4). Lys725 mainly interacts with the phosphate group of the POPC molecules in the presence of the membrane patch (Movie S6), whereas it is moving toward Thr642 in the water, shifting the helix closer to the loop (blue color in Movie S9). The hydrophobic residues Val721 and Phe722 also move into the interior of the pocket to avoid contact with the water reducing the volume of the pocket.

To further validate our assumption about the existence of an equilibrium between a closed and an open state for GVIA iPLA$_2$, SMD simulations were conducted on each of these states. In particular, the PAPC molecule was forced into the pocket of the enzyme, and the extraction force was calculated for each of the states. The SMD simulations showed that the force calculated for the closed state (cyan curve, Fig. S8*B*) is higher than the one calculated for the open state (blue curve, Fig. S8*B*), suggesting that in the case of the closed state, the PAPC probably experiences steric clashes with the residues that prevent its extraction into the binding pocket. The same difference in the extraction force was not observed for GIVA cPLA$_2$ (Fig. S8*A*). For the SMD simulation of GIVA cPLA$_2$, the apo form of the enzyme was used as a closed state, whereas the structure of the enzyme after the MD simulation of the enzyme–PAPC complex was used as an open state. It seems that the deep channel binding pocket in GIVA cPLA$_2$ is entirely controlled by the enzyme and thus does not undergo significant changes in the presence of the membrane patch.

Our MD simulations allow us to observe the existence of two states for GVIA iPLA$_2$: the closed state in the presence of water and the open state in the presence of the membrane, and these two states presumably exist in equilibrium. According to our data, the membrane plays a central role in shifting the conformation of the enzyme to the open state. For GIVA cPLA$_2$ we do not have evidence for two states, although it is possible that they exist.

Discussion

Allosteric Role of the Membrane. Even if PLA$_2$s are widely studied in terms of their kinetics through group-specific activity assays as well as their inhibition by various small organic compounds (1), the mechanics of their association with the membrane is not fully understood. On the other hand, the presence of the membrane renders the kinetics of these enzymes quite challenging because PLA$_2$s display special kinetics that follow the surface dilution model (45, 46). According to this model, the first and most crucial step of PLA$_2$s catalytic cycle is the association with the membrane (step A, Fig. 6), through their interfacial surface to form an enzyme–membrane complex, and thereafter they bind

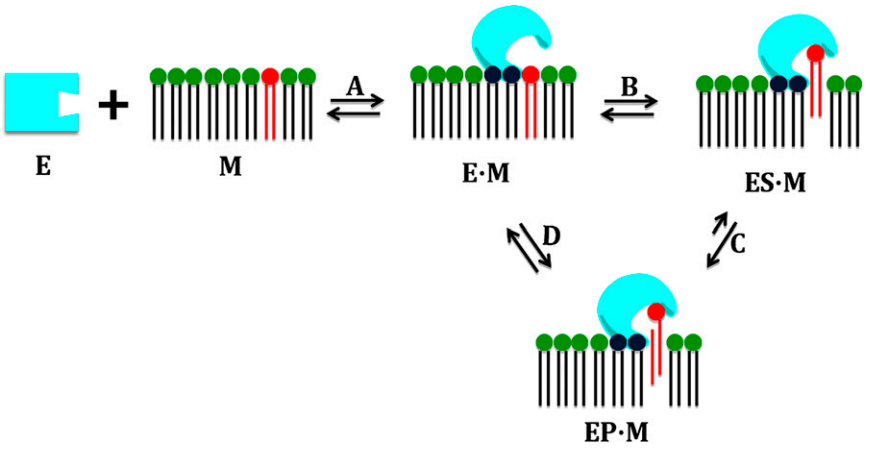

Fig. 6. Representation of the catalytic cycle of phospholipases A_2. (*A*) Membrane association shifts the enzyme conformation from closed to open. (*B*) Extraction and binding of a single phospholipid molecule. (*C*) Hydrolysis of the bound phospholipid molecule. (*D*). Diffusion of the products into the membrane.

a single phospholipid molecule in their binding pocket (step B, Fig. 6). Thus, the interfacial surface is distinctive in terms of topology and function from their binding pocket.

The MD simulations in this study support the notion that the interfacial surface of the PLA_2s contain binding sites for the membrane, which serve as typical allosteric sites (Fig. S8 *C* and *D*). When a PLA_2 enzyme is associated with the membrane, the membrane acts as an allosteric ligand, and thus the enzyme adopts a different conformational state in a way similar to that described by Changeux (47). Contrary to the traditional allosteric model, our enzyme–membrane models suggest that PLA_2s may have more than one allosteric site interacting with the membrane (Fig. S8*D*). Our results show that the volume of the binding pocket of the GVIA $iPLA_2$ is affected to a higher degree by the presence of the membrane patch than the one in GIVA $cPLA_2$. This might be connected to the existence of the C2 domain in GIVA $cPLA_2$, which may be at least partially responsible for the association of the enzyme to the surface of the membrane (30). As a matter of fact, membrane allosteric site(s) might be located on the C2 domain, and the conformational change that the enzyme undergoes might occur in a more time-dependent manner that is not detectable on the time scale accessible to the MD simulations. In the case of GVIA $iPLA_2$, the ankyrin repeats did not show association with the membrane by DXMS, suggesting that the catalytic domain is entirely responsible for the association of the enzyme with the membrane through the residues 708–730 (29). This region was also found to play an important role in the binding of the PAPC. As a result, the binding pocket is in close proximity to the membrane and is affected more by its properties in term of volume and shape. In future studies, we would hope to explore in more detail the effects of varying membrane phospholipid composition on the association of these enzymes with the membrane using these methods.

Extraction and Binding Pocket Specificity of GIVA $cPLA_2$ and GVIA $iPLA_2$. In addition to the allosteric site on the interfacial surface, each PLA_2 contains a binding pocket that is unique in terms of its volume and shape. GIVA $cPLA_2$, for instance, contains a deep channel binding pocket that accommodates the PAPC molecule in its entirety (Fig. S8*C*), whereas GVIA $iPLA_2$ contains a shallower, solvent-exposed pocket. According to the MD simulations, the PAPC molecule did not exhibit any interactions with the POPC membrane in GIVA $cPLA_2$. The PAPC molecule is completely protected and isolated from the rest of the membrane during the entire simulation (Movie S5). This might be connected with the high specificity that GIVA $cPLA_2$ exhibits for AA at the *sn*-2 position of the phospholipid molecule. It is also remarkable that the GIVA $cPLA_2$ pocket contains mostly aromatic residues that might act as a fingerprint recognizing the four double bonds of the *sn*-2 arachidonoyl chain through π-π stacking. The lid exhibits high flexibility during the extraction and binding of the PAPC but remains in close contact with it during the entire simulation, creating a cocoon-like binding pocket that keeps the PAPC protected from water. In other words, GIVA $cPLA_2$ induces complete control of the PAPC binding through the deep channel pocket and its aromatic residues to selectively bind and hydrolyze its substrate (Fig. S8*C*). For the GVIA $iPLA_2$, the MD simulations showed that there is a synergy between the enzyme and the membrane during the binding of the PAPC (Movie S6). The PAPC molecule is in close contact with the POPC molecules of the membrane patch during the MD simulation. This might explain the lack of selectivity at the *sn*-2 position for GVIA $iPLA_2$, whose pocket is affected more by the presence of the membrane (Fig. S8*D*).

Hydrolysis Mechanism. Both enzymes hydrolyze their phospholipid substrate by using a catalytic dyad of Ser/Asp. Therefore, they share a common mechanism for the hydrolysis step (step C, Fig. 6). In Fig. S9, we propose a common mechanism for the hydrolysis of a phospholipid molecule for both enzymes. After the binding of the phospholipid molecule, which is stabilized in the pocket through interactions of its phosphate group with an asparagine and an arginine (GIVA $cPLA_2$) or a lysine (GVIA $iPLA_2$), the aspartic acid abstracts a proton from the catalytic serine, which in turn attacks the carbonyl group of the *sn*-2 position, leading to the formation of the tetrahedral intermediate. The tetrahedral intermediate is instantly stabilized by the oxyanion hole, consisting of two glycines, and is then cleaved leading to a serine-acyl intermediate, with the aspartic acid transferring a proton to the lysophospholipid product. In an analogous manner, the aspartic acid abstracts a proton from a water molecule, generating a hydroxyl anion that attacks the carbonyl group of the serine-acyl intermediate. Finally, the second tetrahedral intermediate collapses to release the fatty acid, whereas the catalytic serine abstracts the proton from the aspartic acid. The catalytic cycle ends with the diffusion of the products in the membrane (step D, Fig. 6). The enzyme–membrane complex is then ready for another extraction and binding of a substrate phospholipid and the subsequent hydrolysis step of the catalytic cycle.

Conclusion

This study provides insight into the catalytic cycle of PLA_2s by using two cytosolic structurally different enzymes. This is, to our knowledge, the first time that GIVA $cPLA_2$ and GVIA $iPLA_2$ are combined in a study in terms of their association with the membrane, the extraction and binding of a phospholipid substrate molecule, and the hydrolysis of the substrate. Our computer-aided techniques guided by previously published experimental DXMS

results (28–31) revealed interesting information about the different role that the membrane plays for these two enzymes. We have also found topological and functional differences in the binding pockets of the two enzymes. All of the above information will be used to rationally design potent and selective inhibitors for these two enzymes that might evolve to future therapeutic agents.

Materials and Methods

A detailed description of the computational methods used in this study is provided in *SI Materials and Methods*. Briefly, the homology model of GVIA iPLA$_2$ was built using the Prime 3.1 protein structure suite programs (34). The X-ray crystal structure of GIVA cPLA$_2$ (PDB ID 1CJY) was prepared using the Protein Preparation Wizard module (48). The GIVA cPLA$_2$ and GVIA iPLA$_2$ binding pockets were identified using SiteMap 2.6 (37). The IFD protocol was used to generate the enzyme–PAPC complexes (32). The MD and SMD simulations were performed using NAMD 2.9 (33), and the results were analyzed using the VMD package (42) and the POVME algorithm (43).

ACKNOWLEDGMENTS. We thank Drs. Robert Konecny and Brain Fox for their help with the Schrödinger suite. This work was supported by NIH Grant GM20501 (to E.A.D.). Work in the J.A.M. group is supported in part by the National Science Foundation (NSF), NIH, Howard Hughes Medical Institute, and NBCR (National Biomedical Computation Resource). Anton computer time was provided by the MMBioS through Grant P41GM103712-S1 from the NIH and the Pittsburgh Supercomputing Center. The Anton machine at PSC (Pittsburgh Supercomputing Center) was generously made available by D.E. Shaw Research. This work used the XSEDE (Extreme Science and Engineering Discovery Environment), which is supported by NSF Grant ACI-1053575.

1. Dennis EA, Cao J, Hsu YH, Magrioti V, Kokotos G (2011) Phospholipase A$_2$ enzymes: Physical structure, biological function, disease implication, chemical inhibition, and therapeutic intervention. *Chem Rev* 111(10):6130–6185.
2. Buczynski MW, Dumlao DS, Dennis EA (2009) Thematic Review Series: Proteomics. An integrated omics analysis of eicosanoid biology. *J Lipid Res* 50(6):1015–1038.
3. Pniewska E, Pawliczak R (2013) The involvement of phospholipases A$_2$ in asthma and chronic obstructive pulmonary disease. *Mediators Inflamm* 2013:793505.
4. Masuda S, et al. (2005) Various secretory phospholipase A$_2$ enzymes are expressed in rheumatoid arthritis and augment prostaglandin production in cultured synovial cells. *FEBS J* 272(3):655–672.
5. Rosenson RS, Hurt-Camejo E (2012) Phospholipase A$_2$ enzymes and the risk of atherosclerosis. *Eur Heart J* 33(23):2899–2909.
6. Nagase T, et al. (2002) A pivotal role of cytosolic phospholipase A(2) in bleomycin-induced pulmonary fibrosis. *Nat Med* 8(5):480–484.
7. Malhotra A, et al. (2009) Role of calcium-independent phospholipase A$_2$ in the pathogenesis of Barth syndrome. *Proc Natl Acad Sci USA* 106(7):2337–2341.
8. Mouchlis VD, et al. (2012) Binding conformation of 2-oxoamide inhibitors to group IVA cytosolic phospholipase A$_2$ determined by molecular docking combined with molecular dynamics. *J Chem Inf Model* 52(1):243–254.
9. Mouchlis VD, Barbayianni E, Mavromoustakos TM, Kokotos G (2011) The application of rational design on phospholipase A(2) inhibitors. *Curr Med Chem* 18(17):2566–2582.
10. Magrioti V, et al. (2013) New potent and selective polyfluoroalkyl ketone inhibitors of GVIA calcium-independent phospholipase A$_2$. *Bioorg Med Chem* 21(18):5823–5829.
11. Kramer RM, Roberts EF, Manetta J, Putnam JE (1991) The $Ca^{2(+)}$-sensitive cytosolic phospholipase A$_2$ is a 100-kDa protein in human monoblast U937 cells. *J Biol Chem* 266(8):5268–5272.
12. Sharp JD, et al. (1991) Molecular cloning and expression of human $Ca^{(2+)}$-sensitive cytosolic phospholipase A$_2$. *J Biol Chem* 266(23):14850–14853.
13. Dessen A, et al. (1999) Crystal structure of human cytosolic phospholipase A$_2$ reveals a novel topology and catalytic mechanism. *Cell* 97(3):349–360.
14. Channon JY, Leslie CC (1990) A calcium-dependent mechanism for associating a soluble arachidonoyl-hydrolyzing phospholipase A$_2$ with membrane in the macrophage cell line RAW 264.7. *J Biol Chem* 265(10):5409–5413.
15. Pickard RT, et al. (1996) Identification of essential residues for the catalytic function of 85-kDa cytosolic phospholipase A$_2$. Probing the role of histidine, aspartic acid, cysteine, and arginine. *J Biol Chem* 271(32):19225–19231.
16. Lin LL, et al. (1993) cPLA$_2$ is phosphorylated and activated by MAP kinase. *Cell* 72(2): 269–278.
17. Nakamura H, Hirabayashi T, Shimizu M, Murayama T (2006) Ceramide-1-phosphate activates cytosolic phospholipase A$_{2}\alpha$ directly and by PKC pathway. *Biochem Pharmacol* 71(6):850–857.
18. Mosior M, Six DA, Dennis EA (1998) Group IV cytosolic phospholipase A$_2$ binds with high affinity and specificity to phosphatidylinositol 4,5-bisphosphate resulting in dramatic increases in activity. *J Biol Chem* 273(4):2184–2191.
19. Clark JD, et al. (1991) A novel arachidonic acid-selective cytosolic PLA$_2$ contains a $Ca^{(2+)}$-dependent translocation domain with homology to PKC and GAP. *Cell* 65(6):1043–1051.
20. Larsson Forsell PK, Kennedy BP, Claesson HE (1999) The human calcium-independent phospholipase A$_2$ gene multiple enzymes with distinct properties from a single gene. *Eur J Biochem* 262(2):575–585.
21. Ma Z, Wang X, Nowatzke W, Ramanadham S, Turk J (1999) Human pancreatic islets express mRNA species encoding two distinct catalytically active isoforms of group VI phospholipase A$_2$ (iPLA$_2$) that arise from an exon-skipping mechanism of alternative splicing of the transcript from the iPLA$_2$ gene on chromosome 22q13.1. *J Biol Chem* 274(14):9607–9616.
22. Michaely P, Tomchick DR, Machius M, Anderson RG (2002) Crystal structure of a 12 ANK repeat stack from human ankyrinR. *EMBO J* 21(23):6387–6396.
23. Balboa MA, Balsinde J, Jones SS, Dennis EA (1997) Identity between the Ca^{2+}-independent phospholipase A$_2$ enzymes from P388D1 macrophages and Chinese hamster ovary cells. *J Biol Chem* 272(13):8576–8580.
24. Lio YC, Dennis EA (1998) Interfacial activation, lysophospholipase and transacylase activity of group VI Ca^{2+}-independent phospholipase A$_2$. *Biochim Biophys Acta* 1392(2-3): 320–332.
25. Percy AJ, Rey M, Burns KM, Schriemer DC (2012) Probing protein interactions with hydrogen/deuterium exchange and mass spectrometry—a review. *Anal Chim Acta* 721:7–21.
26. Harkewicz R, Dennis EA (2011) Applications of mass spectrometry to lipids and membranes. *Annu Rev Biochem* 80:301–325.
27. Cao J, Burke JE, Dennis EA (2013) Using hydrogen/deuterium exchange mass spectrometry to define the specific interactions of the phospholipase A$_2$ superfamily with lipid substrates, inhibitors, and membranes. *J Biol Chem* 288(3):1806–1813.
28. Hsu Y-H, et al. (2013) Fluoroketone inhibition of $Ca^{(2+)}$-independent phospholipase A$_2$ through binding pocket association defined by hydrogen/deuterium exchange and molecular dynamics. *J Am Chem Soc* 135(4):1330–1337.
29. Hsu YH, Burke JE, Li S, Woods VL, Jr, Dennis EA (2009) Localizing the membrane binding region of Group VIA Ca^{2+}-independent phospholipase A$_2$ using peptide amide hydrogen/deuterium exchange mass spectrometry. *J Biol Chem* 284(35):23652–23661.
30. Burke JE, et al. (2008) A phospholipid substrate molecule residing in the membrane surface mediates opening of the lid region in group IVA cytosolic phospholipase A$_2$. *J Biol Chem* 283(45):31227–31236.
31. Burke JE, et al. (2009) Location of inhibitors bound to group IVA phospholipase A$_2$ determined by molecular dynamics and deuterium exchange mass spectrometry. *J Am Chem Soc* 131(23):8083–8091.
32. Suite 2012 (2012) *Schrödinger Suite 2012 Induced Fit Docking Protocol; Glide Version 5.8, Schrödinger, LLC, New York, NY, 2012; Prime Version 3.1* (Schrödinger, LLC, New York).
33. Phillips JC, et al. (2005) Scalable molecular dynamics with NAMD. *J Comput Chem* 26(16):1781–1802.
34. Suite 2012 (2012) *Prime, Version 3.1* (Schrödinger, LLC, New York).
35. Rydel TJ, et al. (2003) The crystal structure, mutagenesis, and activity studies reveal that patatin is a lipid acyl hydrolase with a Ser-Asp catalytic dyad. *Biochemistry* 42(22): 6696–6708.
36. Jenkins CM, et al. (2004) Identification, cloning, expression, and purification of three novel human calcium-independent phospholipase A$_2$ family members possessing triacylglycerol lipase and acylglycerol transacylase activities. *J Biol Chem* 279(47): 48968–48975.
37. Suite 2012 (2012) *SiteMap, Version 2.6* (Schrödinger, LLC, New York, NY).
38. Bucher D, Hsu YH, Mouchlis VD, Dennis EA, McCammon JA (2013) Insertion of the Ca^{2+}-independent phospholipase A$_2$ into a phospholipid bilayer via coarse-grained and atomistic molecular dynamics simulations. *PLOS Comput Biol* 9(7):e1003156.
39. Chen H, et al. (2007) Charge delocalization in proton channels, I: The aquaporin channels and proton blockage. *Biophys J* 92(1):46–60.
40. Wang Y, Schulten K, Tajkhorshid E (2005) What makes an aquaporin a glycerol channel? A comparative study of AqpZ and GlpF. *Structure* 13(8):1107–1118.
41. Karplus M, McCammon JA (2002) Molecular dynamics simulations of biomolecules. *Nat Struct Mol Biol* 9(9):647–653.
42. Humphrey W, Dalke A, Schulten K (1996) VMD: Visual molecular dynamics. *J Mol Graph* 14(1):33–38, 27–28.
43. Durrant JD, de Oliveira CA, McCammon JA (2011) POVME: An algorithm for measuring binding-pocket volumes. *J Mol Graph Model* 29(5):773–776.
44. Zuccotto F, Ardini E, Casale E, Angiolini M (2010) Through the "gatekeeper door": Exploiting the active kinase conformation. *J Med Chem* 53(7):2681–2694.
45. Carman GM, Deems RA, Dennis EA (1995) Lipid signaling enzymes and surface dilution kinetics. *J Biol Chem* 270(32):18711–18714.
46. Deems RA, Eaton BR, Dennis EA (1975) Kinetic analysis of phospholipase A$_2$ activity toward mixed micelles and its implications for the study of lipolytic enzymes. *J Biol Chem* 250(23):9013–9020.
47. Changeux J-P (2012) Allostery and the Monod-Wyman-Changeux model after 50 years. *Annu Rev Biophys* 41:103–133.
48. Suite 2012 (2012) *Schrödinger Suite 2012 Protein Preparation Wizard; Epik Version 2.3, Schrödinger, LLC, New York, NY, 2012; Impact Version 5.8, Schrödinger, LLC, New York, NY, 2012; Prime Version 3.1* (Schrödinger, LLC, New York).